Sea Ice Investigations in the Laptev Sea Area in Late Summer Using SAR Data

by S. Sandven • Ø. Dalen • M. Lundhaug • K. Kloster • V.Y. Alexandrov • L.V. Zaitsev

RÉSUMÉ

La zone de la Mer de Laptev, incluant le détroit de Vilkitsky, constitue un segment important de la route maritime du nord (Northern Sea Route) où la présence de glace de mer rend la navigation difficile, même durant la période estivale. L'objectif de cette étude était donc de démontrer et de valider le potentiel des images RSO à fournir une information précise sur la glace en soutien à la navigation dans la glace, encore prédominante dans cette région à la fin de l'été. Une expérience a été réalisée en août-septembre 1997 basée sur l'utilisation conjointe d'images RADARSAT et RSO d'ERS-2 combinées avec des données d'observations in situ SSM/I acquises par des brise-glaces. Ces données ont été utilisées pour analyser la concentration de glace, les types de glace, la dérive des glaces et d'autres caractéristiques de la glace observées durant cette période. On discute du potentiel des images ScanSAR de RADARSAT et RSO d'ERS dans la détermination de ces paramètres de la glace dans les conditions de fin d'été dans la mer de Laptev. La mer de Laptev de même que d'autres secteurs de la route maritime du nord devraient constituer des secteurs importants pour l'exploration et l'exploitation du pétrole et du gaz dans le futur, ce qui devrait augmenter conséquemment la demande pour un suivi de la glace basé sur les données RSO en soutien à la navigation dans les glaces ainsi que pour le forage et les autres opérations au large.

SUMMARY

The Laptev Sea area, including the Vilkitsky Strait, is an important part of the Northern Sea Route where the presence of sea ice makes navigation difficult even in the summer season. The objective of this study was therefore to demonstrate and validate the capability of SAR imagery to provide accurate ice information to support ice navigation, which is most important in late summer in this region. An experiment was set up in August-September 1997 with joint use of RADARSAT and ERS-2 SAR images combined with SSM/I data in situ observations from icebreakers. These data were used to analyze ice concentration, ice types, ice drift and other ice features present in this period. The capability of RADARSAT ScanSAR and ERS SAR images to determine these ice parameters during late summer conditions in the Laptev Sea area is discussed. The Laptev Sea as well as other parts of the Northern Sea Route are expected to become important areas for future oil and gas exploration and exploitation, which will increase the demand for SAR ice monitoring to support ice navigation, drilling and other offshore operations.

INTRODUCTION

The Laptev Sea area, which is an important part of the Northern Sea Route (NSR), is bounded by the Severnaya Zemlya Archipelago in the west and by the New Siberian Islands in the east (**Figure 1a**). By the end of October a belt of fast ice starts to form along the Siberian coast. Floes of second-year ice can be embedded into the fast ice during formation in the autumn (Reimnitz *et al.*, 1995). Recurring flaw polynyas are typical for the winter Laptev Sea where new ice is pushed away from the fast ice by wind drift and ocean currents (Zakharov, 1966; Dmitrenko *et al.*, 1999). During autumn, winter, and spring, sea ice in the Laptev Sea has a net drift northward to the Arctic Ocean, whereas the ice circulation is more variable in summer (Zakharov, 1966; Gudkovich *et al.*, 1972). During the period 1979-1995 the average winter ice outflow amounted to 483 000 km^2, whereas on average 40 000 km^2 of sea ice were imported in summer through the northern boundary (Alexandrov *et al.*, 2000). Ice melting starts in late May or early June centred around the flaw polynyas. The Taimyr ice massif usually persists throughout the summer and can even widen in some years because of southward ice drift and may therefore block coastal routes with thick ice. Icebergs, calving from Severnaya Zemlya outlet glaciers, can frequently be observed in the western part of the Laptev Sea including the Vilkitsky Strait (Govorukha, 1988; Eicken *et al.*, 1994; Abramov, 1996; Zakharov, 1996).

Regular navigation in the Laptev Sea is limited to the summer season, because winter navigation requires icebreakers of the Arktika type, with more than 65000 horsepower, and even these icebreakers can have problems operating under difficult ice conditions. Therefore high-resolution radar images are particularly important for supporting navigation in this area.

Manuscript received: 26 January 2001 / Revised: 6 June 2001.

• S. Sandven, Ø. Dalen, M. Lundhaug and K. Kloster are with the Nansen Environmental and Remote Sensing Centre, Edvard Griegsvei 3a, N-5059, Bergen, Norway, Tel: 47 55 29 72 88; Fax: 47 55 20 00 50, E-mail: stein.sandven@nrsc.no.

• V.Y. Alexandrov and L.V. Zaitsev are with the Nansen International Environmental and Remote Sensing Centre Ul. Bolshaya Monetnaya, 26/28, 197061, St. Petersburg, Russia Tel: 7 (812) 234 39 24; fax: 7 (812) 234 38 65 E-mail: vitali.alexandrov@niersc.spb.ru.

Sea ice charts have been produced for several decades based mainly on aircraft observations and optical satellite images. Satellite radar observations started in 1983 with Okean Side-Looking Radar images (Bushuev *et al.*, 1985). Since 1991, a series of ice monitoring experiments using ERS SAR images have been carried out by Nansen Centers in Bergen and St. Petersburg together with Murmansk Shipping Company. During these experiments SAR images were transmitted by INMARSAT to icebreakers to support ice navigation (Johannessen *et al.*, 2000). With ERS SAR images it is possible to identify icebergs, several ice types and phenomena, which can be dangerous for icebreakers (Johannessen *et al.*, 1997; Kolatschek *et al.*, 1995; Sandven *et al.*, 1999). RADARSAT ScanSAR data have been used by the Nansen Center to observe sea ice in the Kara Sea region during winter conditions, described by Alexandrov *et al.* (2000).

In this paper, we will demonstrate uses of ScanSAR images, supported by some ERS-2 SAR images, for sea ice monitoring in late summer conditions, which is the most important period for the ship traffic. SAR signatures of late summer ice types, ice drift and other features have been analyzed and a SAR ice concentration algorithm has been tested and compared with *in situ* ice observations from icebreakers and helicopter. Also ice drift vectors are estimated from consecutive images and used to discuss current- and wind-driven ice motion in the study area.

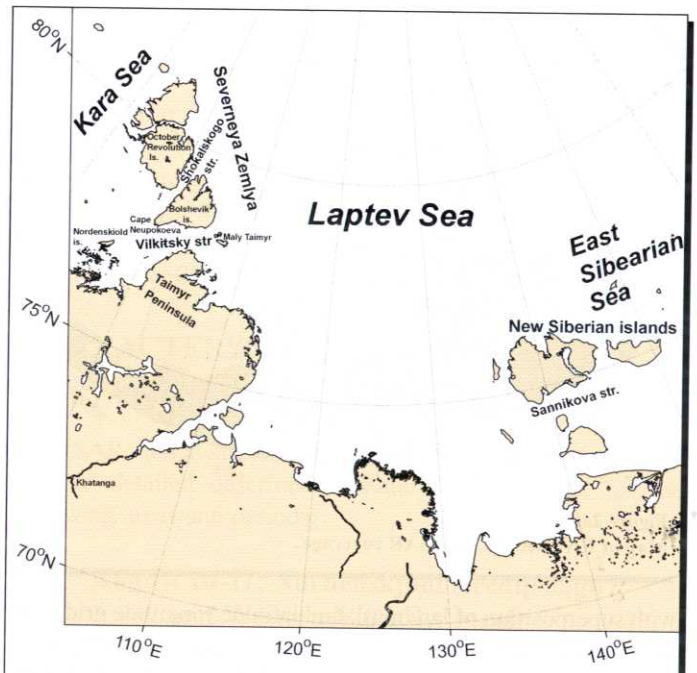

Figure 1a.
Map of study area with some geographical names.

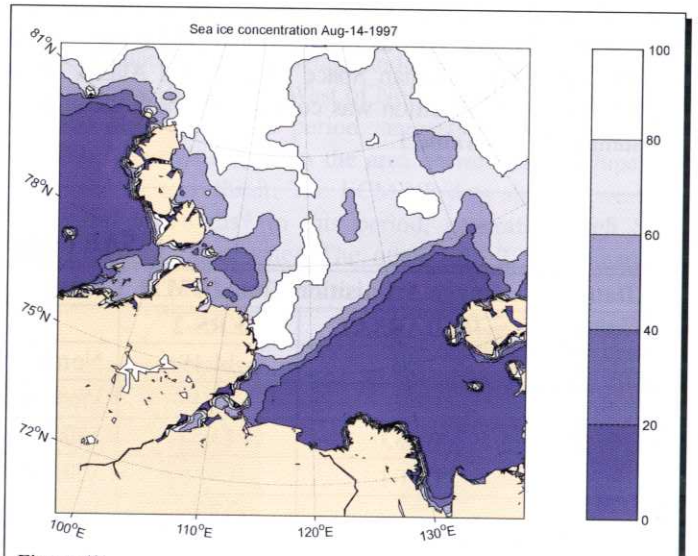

Figure 1b.
SSM/I-derived ice concentration in % for August 14 1997.

Data Acquisition and Icebreaker Expedition

Use of Passive Microwave Satellite (SSMI) Data

To observe the general ice conditions before and during the expedition, SSM/I data were obtained in near-real time and maps of ice concentration were prepared using the NORSEX algorithm (Svendsen *et al.*, 1983) modified for use with the 85 Ghz channel. By using this channel it is possible to obtain higher resolution and more accurate localization of the ice edge and reduce the errors near land. A series of SSM/I ice concentration maps, covering the period of four weeks from August 10, provided an overview of the ice extent and concentration in the study area. The predominant features were the large open water areas in the northeastern Kara Sea and the southern Laptev Sea (**Figure 1b**). The Taimyr ice massif extended southward to the Taimyr coast at a concentration of 80% and more, acting as a barrier for ships sailing from Vilkitsky Strait to the Laptev Sea. The position of this ice massif changed very little in the four week period when data when SSM/I data were analyzed. The ice concentration in the Vilkitsky Strait area was initially about 50% and decreased to less than 20% at the end of the period. The large open water areas persisted in the Kara Sea and the southern Laptev Sea throughout the period (**Figure 1b**).

Acquisition and Processing of SAR Data

The acquired RADARSAT ScanSAR scenes covered the Vilkitsky Strait area and parts of the Laptev and East-Siberian Seas over the period from August 14 to September 7 (**Figure 2a**). Several ERS-2 SAR images were acquired in the Vilkitsky Strait area to supplement the RADARSAT images and obtain more frequent temporal sampling (**Figure 2b**). SAR images for the western part of the Laptev Sea were obtained from Tromsø Satellite Station (TSS) in near-real time (3-4 hours delay) and delivered on Internet to the Nansen Center in Bergen. The area west of about 105°E is situated within the station mask of TSS. After the images were geocoded and contrast enhanced

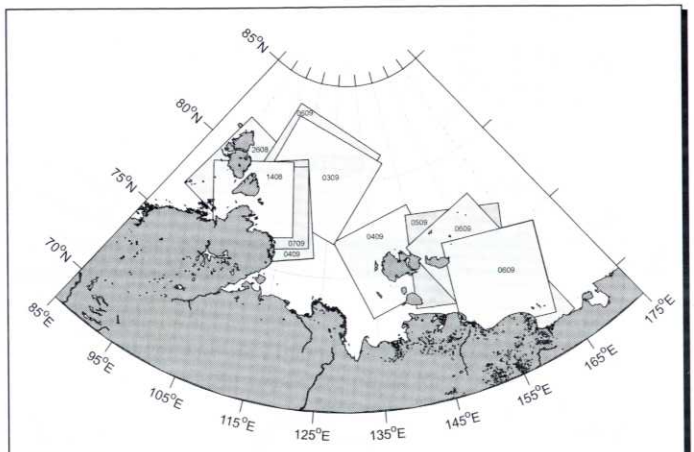

Figure 2a.
Map of RADARSAT ScanSAR coverage.

with superposition of landmask and latitude/longitude grid, they were transmitted to Murmansk Shipping Company's Headquarters for planning of the expedition and onboard the icebreaker after she left port. Typical turnaround time from SAR acquisition to delivery onboard icebreakers was about six hours. For the central part of the Laptev Sea and the area around the New Siberian Islands, only archived RADARSAT images could be obtained from Canadian Space Agency and Alaska SAR Facility after the expedition was completed. The SAR images are summarized in **Table 1**.

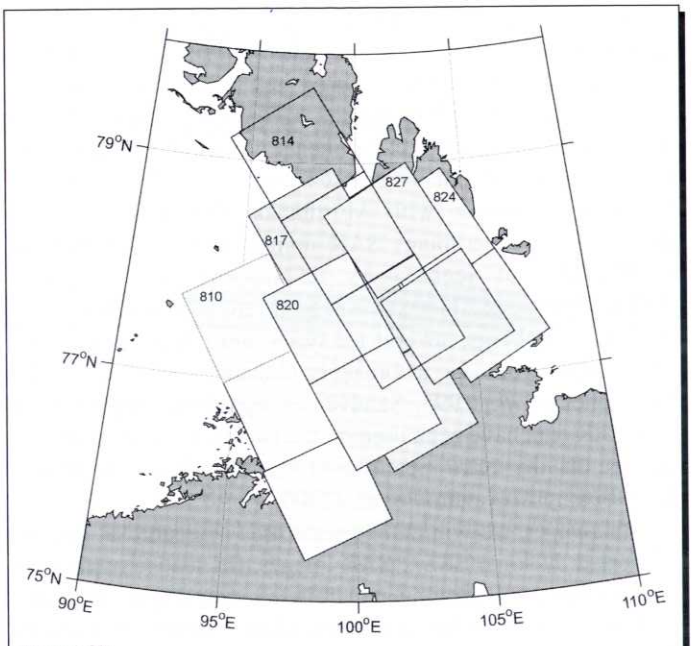

Figure 2b.
Map of ERS-2 SAR coverage. The figures indicate day-month of the SAR scenes.

Data Transmission to I/B Sovetsky Soyuz

I/B Sovetsky Soyuz left Murmansk on September 7 and arrived in the Laptev Sea three days later for supporting ice navigation to Khatanga. The ScanSAR image for September 7

Table 1.
SAR images used in the study.

Date	Image Acquisition Time (GMT)		Area	Receiving Station
	RADARSAT	ERS-2		
10.08		14:19	Nordenskiold archipelago	TSS
11.08		13:48	West Vilkitsky Strait	TSS
14.08	09:33	13:54	Vilkitsky strait area and western Laptev Sea	TSS
15.08	09:04		Vilkitsky strait area and western Laptev Sea	TSS
17.08		13:59	West Vilkitsky Strait	TSS
20.08		14:05	West Vilkitsky Strait	TSS
24.08		13:40	Central Vilkitsky Strait	TSS
26.08	00:30		Vilkitsky strait area and western Laptev Sea	ASF
27.08		13:45	Central Vilkitsky Strait	TSS
31.08	09:37		Vilkitsky strait area and western Laptev Sea	TSS
03.09	23:22		Central - northern Laptev Sea	ASF
04.09	21:12		New Siberian Islands - north/east	ASF
04.09	07:39		New Siberian Islands - north/west	Gatineau
04.09	09:20		Vilkitsky strait area and western Laptev Sea	Gatineau
05.09	20:44		New Siberian Islands - east	ASF
06:09	20:15		New Siberian Islands - east	ASF
06.09	06:39		New Siberian Islands - east (2 ScanSAR scenes)	Gatineau
06.09	23:34		Central - northern Laptev Sea	ASF
07.09	09:33		Vilkitsky strait area and western Laptev Sea	TSS

and several SSM/I ice concentration maps were transmitted onboard the icebreaker via INMARSAT and used for planning of sailing routes. The pixel size of the RADARSAT image was averaged to 500 x 500 m and JPEG compression was applied to obtain a reasonable file size, less than 1 Mbyte, which could be transmitted in a few minutes. Scientists from the Nansen Center in St. Petersburg received SAR and SSM/I data onboard the icebreaker and collected *in situ* ice observations for support of the SAR ice analysis.

Meteorological Data

In the western Laptev Sea area covered by SAR imagery, visual ice observations were obtained from the bridge of the icebreakers and from helicopter ice reconnaissance flights. Sea ice and meteorological data were collected several times per day while the icebreaker operated in ice areas. The meteorological observations included air pressure, wind velocity and direction, sea surface and air temperature. In the 10-day period when I/B Sovetsky Soyuz and I/B Yamal operated in the Laptev Sea, the weather conditions were stable and the sea surface temperature was at the freezing point (-1.8° C) allowing formation of new ice in open water areas. Air temperature varied from typically -3° C at night to +1° C in daytime. The wind speed was moderate, not exceeding 10 ms^{-1}, which generally agreed with the European Center for Medium Range Weather Forecasts (ECMWF) data, which were analyzed after the expedition.

Preprocessing of the SAR Images

Since the RADARSAT data were obtained from three receiving stations, TSS in Norway, Gatineau in Canada and Alaska SAR Facility, it was necessary to preprocess the images to obtain a set of relatively homogeneous ScanSAR images that could also be compared with the ERS-2 images. For ERS-2 SAR data delivered by TSS as Low-Resolution Images (LRI) there is a standard procedure for correction of the three effects: antenna gain, slant range and incidence angle. A calibration procedure for ERS SAR data is established, which also relates corrected pixel values to σ_0, based on a calibration constant from previous sea ice investigations (Sandven *et al.*, 1999). This procedure gives an accuracy of the σ_0 values within approximately 1 dB. For RADARSAT data, a common calibration procedure for the three ground stations was not available for the images used in this study. It was not possible to obtain an accurate calibration constant for the RADARSAT images from TSS, but the pixel values were provided as a linear function of log σ_0 after correction for incidence angle. The RADARSAT images received from CSA and ASF had pixel values proportional to $(\sigma_0)^{0.5}$ after incidence angle correction, with the calibration constant given in a range varying Look-Up Table (LUT) (RADARSAT, 1997). Since the accuracy of the LUT was unknown, σ_0 values could have inaccuracy of several dB. Calibration of ASF data was also unknown, but the coding was assumed to be similar to the CSA data. Therefore RADARSAT images with range-corrected pixels, but without absolute calibration, were used in the subsequent analysis. Focus of the study has therefore been on ice features and dynamics that only need pattern recognition and relative backscatter difference between water and ice types.

An important point is that wide-swath SAR images have large variations of σ_0 across the full swath for most surfaces, and in particular for water. For ScanSAR, σ_0 may be up to 15 - 20 dB lower in far-range compared to near-range. All images used in this study were therefore multiplied by a pre-defined range-normalization function, $(\tan\theta)^{\beta}$ where θ is incidence angle. For most ice types β is about 1.5, while for open water it is near 4.

Characterization of Ice Conditions from SAR Data

With SAR data available since early August, it was possible to provide detailed description of the ice conditions for the following areas and periods:

August 10-11: Nordenskjold Archipelago and Western Vilkitsky Strait

SSM/I data from August 10 and onward showed ice concentration above 50% in the area of Nordenskjold archipelago and western Vilkitsky Strait (**Figure 1b**). Also the ERS-2 SAR image of the same day showed the presence of compact ice which drifted eastward, and open water areas near the coast, within the archipelago and in the northwestern corner of the image (**Figure 3**). West of Nordenskjold archipelago no ice was observed in this period, suggesting that the eastward drifting ice originated from the area between the archipelago and the Vilkitsky Strait. The ECMWF data showed westerly winds up to 10 ms^{-1} in this period, generating high SAR backscatter of open water. The other ERS-2 SAR image in

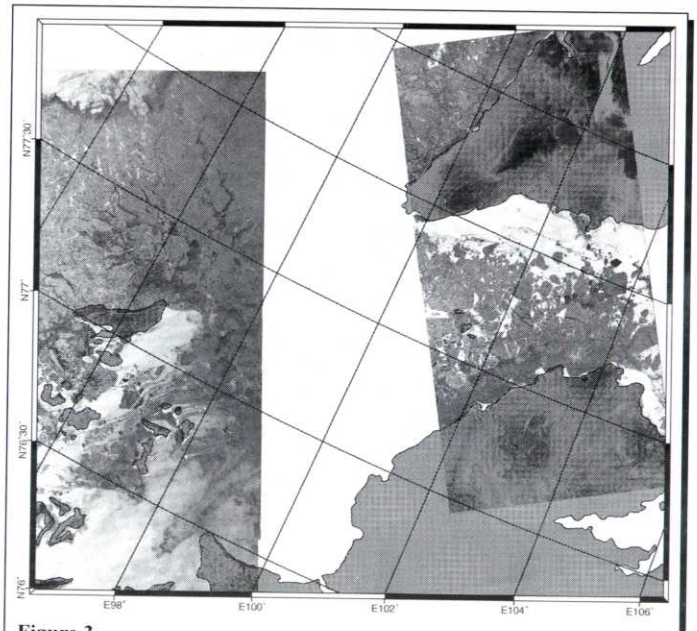

Figure 3.
ERS-2 SAR imagery of the Nordenskjold Archipelago (left swath) on August 10 and Vilkitsky Strait (right swath) on August 11, 1997 ©ESA/TSS, 1997.

Figure 3, obtained on August 11, showed a stream of eastward drifting ice floes in the central and southern part of the Vilkitsky strait, whereas its northern part was mainly ice free.

August 14-17: First ScanSAR Survey of Vilkitsky Strait Area and Western Laptev Sea

The first ScanSAR survey, obtained on August 14 (**Figure 4**), showed that the ice edge in the eastern part of the Kara Sea is clearly visible due to the brighter SAR signatures of open water as compared to the ice covered areas. The wind speed of 5-10 ms^{-1} in this region was sufficient to generate this high backscatter. The eastward ice drift in the Vilkitsky Strait was composed of ice from southwest along the Taimyr coast, and from the northwestern side of Bolshevik Island, where the fast ice of Shokalsky strait started to break up and drifted southward. The eastbound surface current through the Vilkitsky Strait formed a wedge of low concentration ice which penetrated into the Taimyr ice massif. Most of the western Laptev Sea area shown in the image was covered by compact thick ice characterized by relatively high backscatter, whereas the dark SAR signature east of Severnaya Zemlya could be explained by open water during calm wind or the presence of nilas or grease ice. One day later, on August 15, another ScanSAR scene was obtained over almost the same area, allowing estimation of mean ice drift over a period of about 24 hours. In the Laptev Sea, ice drifted in a southeasterly direction at a mean speed of 0.20 ms^{-1}, and in the eastern Vilkitsky Strait an ice displacement of 38 km was found corresponding to a mean speed of 0.44 ms^{-1}. West of the Vilkitsky Strait the winds in the period were west-southwesterly, 5-10 ms^{-1}, and air temperatures varied between 0° and -2°C, according to ECMWF data. East of Severnaya Zemlya, the westerly winds can be reduced by topographic effects, allowing open water to have the lower SAR signature in this area.

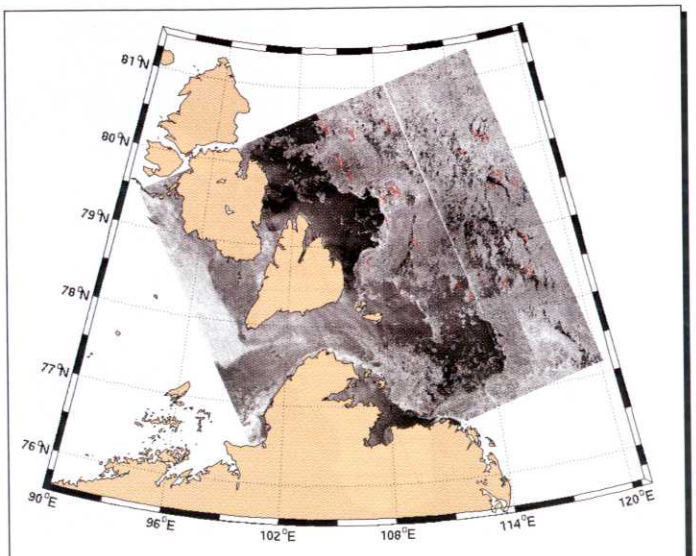

Figure 4.
RADARSAT ScanSAR image of August 14, 1997, with ice drift vectors and land mask superimposed. The mean ice drift speed, estimated between repeated ScanSAR images on August 14 and 15, is about 0.20 ms^{-1}. ©Canadian Space Agency, 1997.

The western part of the Vilkitsky Strait including the area between Bolshevik Island and October Revolution Island, was covered with three consecutive ERS-2 images from August 14 and 20 (**Figure 5**). Similar to the ScanSAR image, the ERS images showed that the ice north and west of Cape Neupokoeva (78°N 100°E) drifted southward into the Vilkitsky Strait and then merged with the eastward flowing ice coming from southwest. A

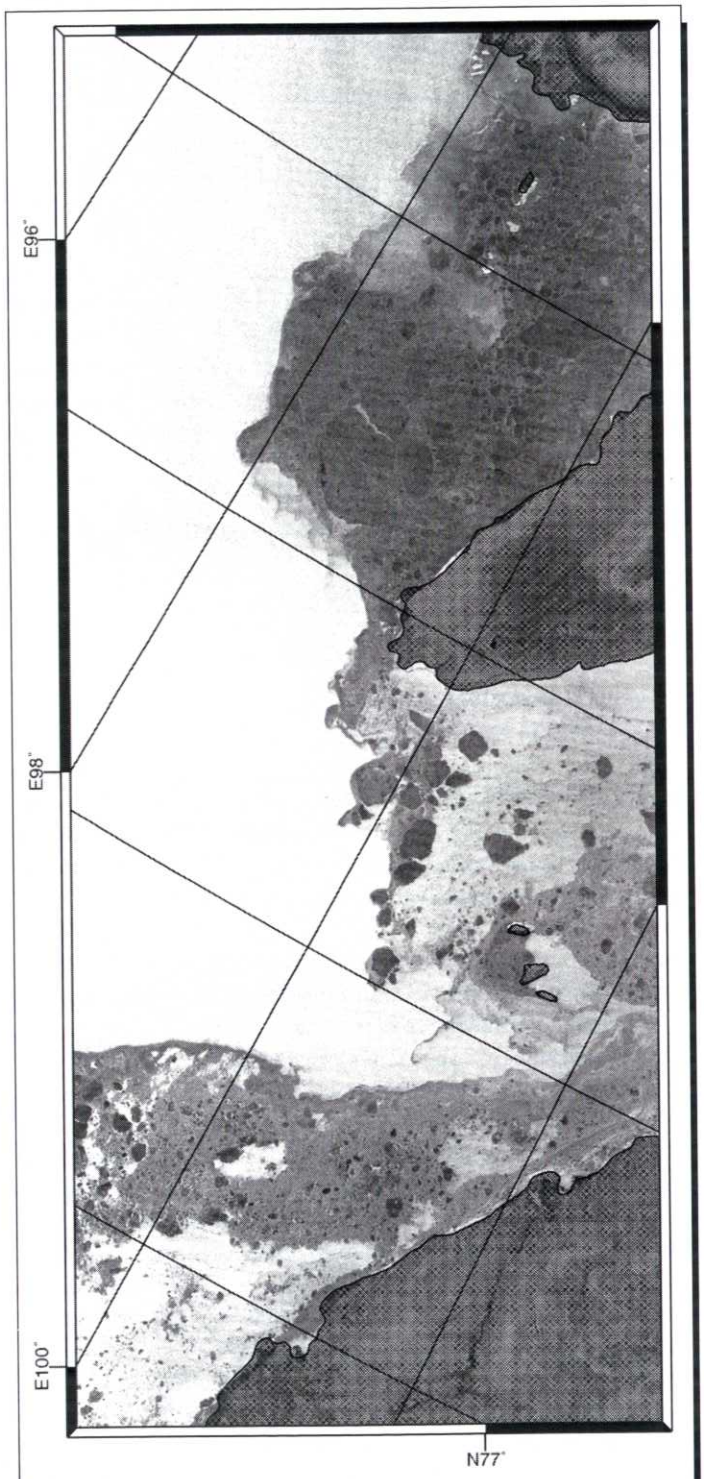

Figure 5.
ERS-2 SAR imagery of western Vilkitsky Strait and parts of Shokalski Strait on August 17, 1997. ©ESA/TSS, 1997.

cluster of 5-10 km large floes observed north of the cape on August 14 had moved about 60 km and was located south of the cape three days later, corresponding to a mean drift speed of 0.23 ms^{-1}. A 25 km large floe, which was located northwest of the cape on August 14, moved 20 km to the southeast in the same period, corresponding to a mean drift speed of 0.08 ms^{-1}. The ice along the Taimyr coast also drifted eastward, as can be recognized by open water on the leeward side of the small islands. The floe displacement in this region between August 17 and 20 suggested a mean drift speed of 0.03 ms^{-1}.

August 26 - 31: Repeated ScanSAR Survey of Vilkitsky Strait and Western Laptev Sea

The ScanSAR image for August 26 (not shown) indicated a reduction of the ice in the Vilkitsky and Shokalsky straits, as compared with the previous ScanSAR survey, and several well-developed ice edge eddies and vortex pairs in the region west of the 100° E longitude. Ice edge eddies and vortex pairs have previously been studied in the Greenland Sea (Johannessen *et al.*, 1994), where mixed barotropic/baroclinic instabilities of the currents were found to be probable generating mechanisms for these phenomena. In the western Laptev Sea, the thick icepack drifted to the southwest at a speed of 0.05 ms^{-1}, while open water/new ice areas persisted east of Severnaya Zemlya.

Ice drift in the Vilkitsky Strait was estimated from SAR images for August 24, 26 and 27. The first image pair showed that two floes located near the northern coast of the strait moved to the south at 0.06-0-08 ms^{-1} in a period of easterly winds (**Figure 6**). In the central part of the strait, floes moved eastward at speeds up to 0.17 ms^{-1} even if the winds continued to be easterly 4-8 ms^{-1}. This suggests that the floes were captured by the eastbound currents which appear to dominate in the central and southern part of the strait.

September 3-6: ScanSAR Coverage of More Ice Areas in Western Laptev Sea and Around New Siberian Islands

Two ScanSAR images for September 3 and 6 (not shown), which were obtained over a central part of the Laptev Sea, were used to estimate a southeasterly ice drift with a mean speed of 0.15 ms^{-1}. Several ScanSAR images, obtained in the area of the New Siberian islands and parts of the East Siberian Sea, were used to make a mosaic and to calculate ice drift for the period September 3 to 6 (**Figure 7**). The mosaic shows that the area to the northeast of the New Siberian Islands and a 100-200 km wide zone along the coast in the East-Siberian Sea were ice free. Scattered ice was found in the New Siberian Straits and to the south of the islands. A diffuse ice edge extending from the east Siberian coast (at 162°E) to the north of the islands is clearly evident the mosaic. Ice concentration increased into the ice massif reaching 90-100% in the northeastern corner of the images.

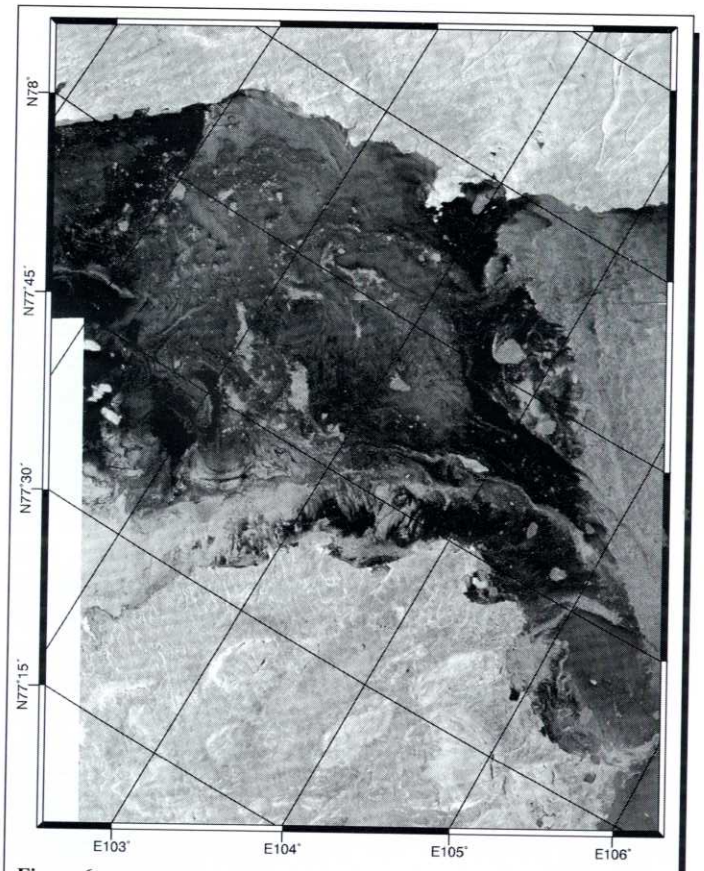

Figure 6.
ERS-2 SAR imagery of the central Vilkitsky Strait on August 27, 1997. The image is composed of two consecutive scenes. ©ESA/TSS, 1997.

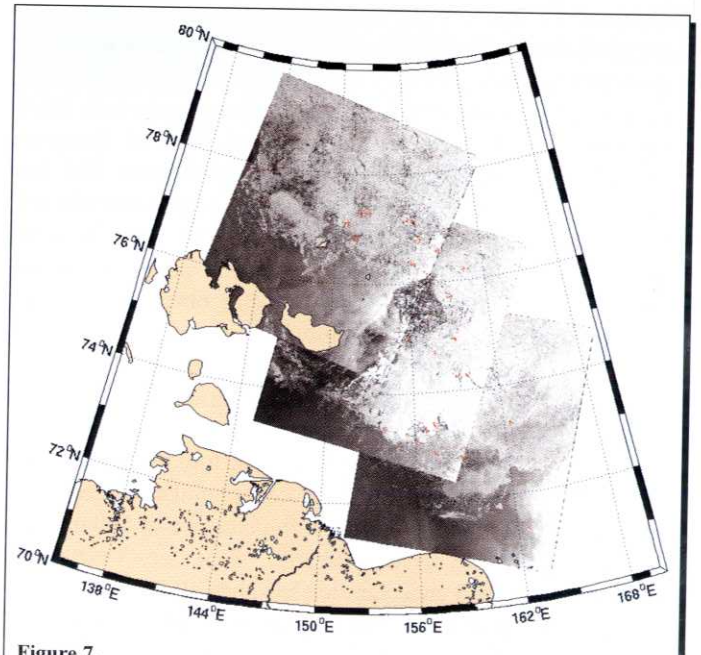

Figure 7.
Mosaic of three RADARSAT ScanSAR images taken in the area of New Siberian Islands from September 3 to 6, 1997, with ice drift vectors superimposed. The mean ice drift speed, estimated between repeated ScanSAR images varies from 0.10 to 0.20 ms^{-1}. ©Canadian Space Agency, 1997.

Validation of SAR Ice Observation Using Icebreakers

The most appropriate ScanSAR image for validation was obtained on September 7. I/B Sovetsky Soyuz operated in the area covered by this image during September 10-11, giving a time-delay of 3-4 days between image acquisition and ship observations. A subset of the September 7 image with superimposed ship track of I/B Sovetsky Soyuz is shown in **Figure 8a**. A series of photographs (**Figure 9**), ice log reports, ice charts from helicopter and meteorological observations taken from the icebreakers were used for this validation. Unfortunately, it was not possible to obtain RADARSAT images after this date, because the satellite went into another mode of operation for monitoring of the Antarctic ice cap.

Due to quiet weather conditions, with temperatures below freezing wind speed from 3-6 ms^{-1}, we assumed that the properties which have an impact on the SAR signatures, such as surface roughness and temperature, snow cover, and salinity of the Taimyr ice massif did not change much in this period. However, the currents observed within and eastward of the Vilkitsky Strait (**Figure 4**) suggested that patches and stripes of first-year ice in the validation area drifted in a southeastward direction. With persistent air temperature between -2°C and -6°C in the period September 2-16 and water temperature at the freezing point, formation of new ice was assumed to take place throughout this period. Our study attempted to provide an overall description of the ice signatures in the SAR image, being aware that validation of new ice areas is more difficult due to the freezing conditions in the period.

The area west of 110° E, between points A and C, was dominated by open water and new ice, which appear as homogeneous grayish signatures in the SAR image (**Figure 8a**) mixed with scattered patches and bands of brighter signature caused by clusters of ice floes. At site A, photographs were taken of pancake ice (**Figure 9a**) and scattered floes of first-year surrounded by open water and grease ice (**Figure 9b**). Ice observers on the icebreaker reported a total ice concentration of 20-30%, of which 10-20% were first-year ice and the same amount of pancake ice (**Table 2**). Between points A and B, several bands of thick first-year ice were observed, and the largest of them can be seen as bright line features against darker background. Ice concentrations in this area were up to 50 %, and the ice mainly consisted of a mixture of grease ice and pancake ice (pancake size up to 1 m), with patches of smaller FY ice floes which were observed continuously Due to low wind velocities (3-4 ms^{-1}) open water had low backscatter similar to grease ice and nilas. The backscatter image, with pixel size of 500 m, also had difficulty identifying first-year ice when floes were small (less than 100 m) and concentration less than 10-20 %.

An iceberg which was about 100 m in horizontal scale was observed from the icebreaker near B at position 77° 25'N 109°19'E. This iceberg can be seen as a bright spot in the full-resolution blow-up of the ScanSAR image (**Figure 8b**). The position of the iceberg observed from the icebreaker four days later is marked by the cross in **Figure 8b**. The time difference of these observations, combined with the position accuracy of

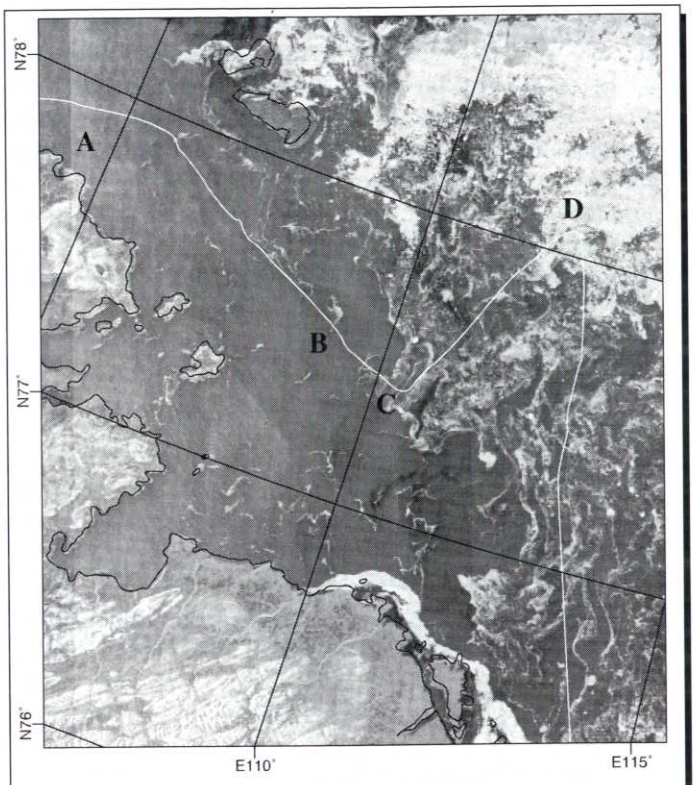

Figure 8a.
Subset of RADARSAT ScanSAR image on September 7, showing the area east of Vilkitsky Strait. The line marks the track of I/B Sovetsky Soyuz which sailed in the areas on September 10 - 11. The points A- D mark different characteristic ice conditions documented by observations onboard the icebreaker. ©Canadian Space Agency, 1997.

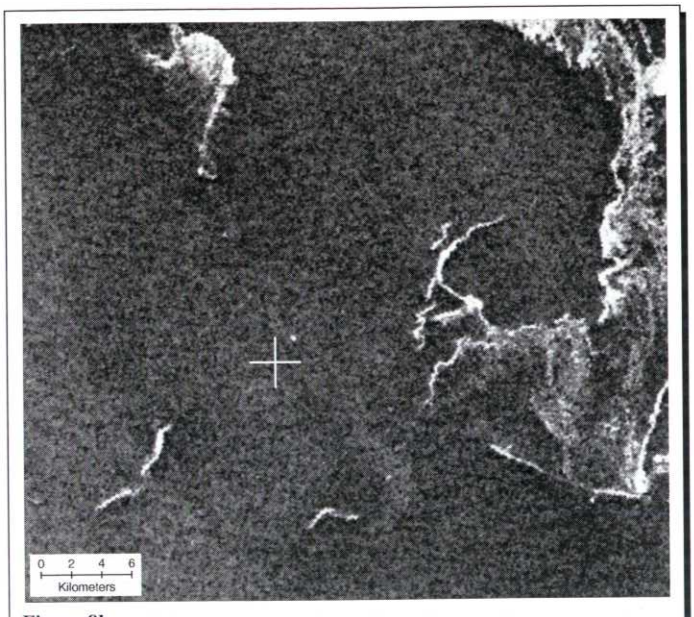

Figure 8b.
Zoomed subimage in full resolution (pixel size 100 m) of the area between B and C, showing the location of a small iceberg (white dot) near the cross which is the position of observation by icebreaker four days after SAR acquisition. The iceberg has a horizontal scale of about 100 m. ©Canadian Space Agency, 1997.

Figure 9.
Photographs of different ice conditions observed by I/B Sovetsky Soyuz on September 10 - 11 within the SAR image of September 7. Pictures a and b were taken at point A in Figure 8, showing pancake ice and scattered floes of first-year ice, respectively. Pictures c and d at point C, where nilas covered up to 80-90 % of the ice area. Pictures e and f were taken at point D where up to 1.5 m thick first-year ice dominated. I/B Sovetsky Soyuz had a rendez-vous with I/B Yamal (picture f) at this position.

Table 2.
Ice and weather observations on September 10 – 11.

Date	Time*	Site & Photo No.	Latitude	Longitude	Observed Ice Concentrations					Meteorological data		
			(N)	(E)	Total	FY-ice	Nilas	Pancake	Grease	Wind direction	Wind speed	Temp.
10.09	10:35	a, b	77°55`	104°20'	30	10 -20		10-20		300	3	- 3
11.09	00:00		77 56	105°31'	30	10 -20		10-20		240	4	-4
	00:40		77°54'	106°02'	90-100	0 - 10		40-50	30 - 40			
		iceberg	77 25	109 19								
	06.42	c, d	77°37'	111°01'	80-90		80-90					
	08.00		77 58	111 47	70-80	10	60-70			180	6	0
	09:00	e, f	78 05	112 05	80-90	70-80	10			180	7	+ 1
	13.30		77 43	112 51	60-70	10-20	50					
	15.00		77 20	113 00	70-80	10-20	50	10				
	16.20		76 57	113 24	60-70	30	30-40			200	9	- 1

* Moscow time = GMT + 3 hours

the image, suggests that the displacement of the iceberg is small, less than 2 km. Furthermore, this suggests that the iceberg is not located in the core of the southeastward coastal current in this area. Other icebergs were not observed in this expedition, but icebergs originating from the Severnaya Zemlya glaciers are not unusual in this region (Alexandrov and Kolatschek, 1997).

Following the icebreaker track east of 110° E, starting at point C (**Figure 8a**), ice concentration generally increased to more than 60-70%, most of it was nilas which can be partly rafted (**Figure 9c**) and mixed with floes of first-year ice (**Figure 9d**). At the northernmost position in the expedition (point D at 78° 05' N, 112° 05' E), patches of nilas and open water occurred between first-year ice with concentration of 80-90%. The floe size increased to 50-200 m and the thickness to 100-150 cm. Typical ice concentration in Taimyr massif was 80-90%. The SAR signature of the first-year ice was relatively bright. Individual floes larger than a few kilometres could be identified. Following the icebreaker track south of 78° 00'N, the ice cover was again characterized by up to 50% concentration of grease ice, nilas and pancakes, while the fraction of first-year was down to 10-20%.

The ScanSAR image of September 4 extended further south between 115° and 120°E as compared with the September 7 image, covering an area of the Taimyr ice massif which was mapped in detail by helicopter surveys on September 10. A subset of the September 4 image is shown in **Figure 10a**, indicating the area mapped by helicopter as well as points of *in situ* ice observations from I/B Yamal. Note that I/B Yamal was sailing through the area on September 4 - marked by the dashed line in the ice chart (**Figure 10b**), which was produced six days later from helicopter surveys. The ice map was produced using standard Russian ice symbols (see Appendix A), indicating ice concentration (in tenths) of the two main ice types, including floe size, thickness/development stage and roughness index. The ice map covers a band of the Taimyr ice massif, which extended toward the coast at 114° E and south of 76°30'N. This ice band, with concentration of 9-10 tenths, moved eastward 20-30 km over the six day period by comparing its location in the SAR of September 4 and the ice map of September 10. The *in situ* observations from I/B Yamal from September 3, 4 and 5 were used to validate the ice concentration analysis described later herein.

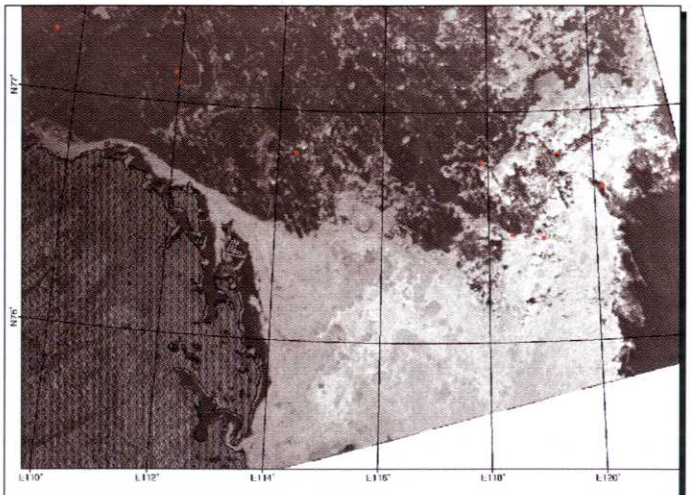

Figure 10a.
Subset of RADARSAT ScanSAR image on September 4, showing the area east of Vilkitsky Strait where the Taimyr ice massif reaches the mainland coast. The dots mark positions were ice observations were obtained by I/B Yamal at the same time as the SAR image. Figure 10b shows the location of the ice chart. ©Canadian Space Agency, 1997.

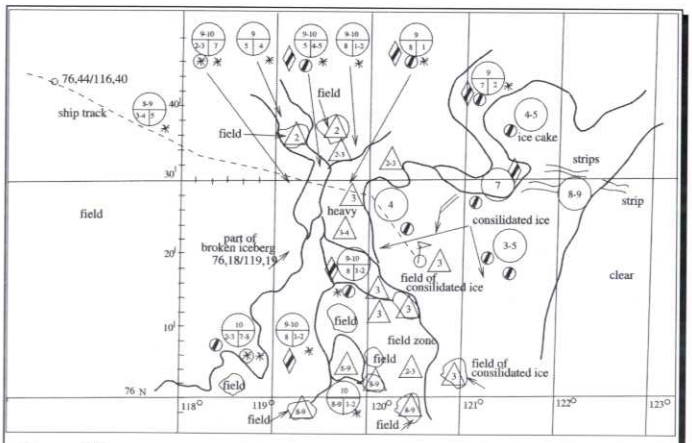

Figure 10b.
Ice chart provided by I/B Yamal on September 4, based on helicopter surveillance. The ice chart uses Russian ice symbols, shown in Appendix A. ©Canadian Space Agency, 1997.

Example of Comparison of RADARSAT and ERS Data

Near simultaneous coverage of the same ice area with both RADARSAT and ERS-2 SAR was only obtained on August 14, when the western Vilkitsky Strait and Shokalsky Strait were mapped by ERS-2 at 1354 GMT and by RADARSAT at 0933 GMT. A subset of the RADARSAT image was extracted covering the same area as the ERS-2 image (**Figure 11**). Both images cover incidence angles from 20° to 26° and have been prepared using the "ice" Look-Up Table discussed earlier. The Look-Up Tables are range-normalizing functions designed to give homogeneous backscatter in range direction for an homogeneous ice surface. For RADARSAT the radiometric resolution is constant at about -0.37dB per pixel. For ERS-2 it is varying from about -0.2 dB per pixel at pixel value of 40 to about -0.1 dB per pixel at pixel value of 80. The pixel size of the two images shown in **Figure 11** was 100 m for ERS-2 and 500 m for RADARSAT. In the subsequent analysis the ERS-2 pixels were averaged to 500 m to allow pixel-by-pixel comparison.

A general characterization of the ice conditions in this area has been briefly described, but due to lack of any *in situ* observations, a clear definition of the ice types cannot be given. Since the RADARSAT image is not absolutely calibrated, we have chosen two methods for comparison of the ERS-2 and RADARSAT images:

1) Six areas each with relatively homogeneous backscatter levels were selected by zig-zag lines for pixel-by-pixel comparison (**Figure 12**), and

2) Other smaller areas where the two data sets give obvious different backscatter are described qualitatively.

The open water area (W1) is clearly identified as a relatively bright area on the left side in both images. The wind was westerly 5 - 10 ms^{-1} which is sufficient to give open water higher backscatter than most ice types in ERS-2 images, as discussed by Sandven *et al.* (1999). Also RADARSAT gives higher backscatter for this open water area compared to other parts of the image. In the northern part of the Vilkitsky Strait (W2) the ERS-2 image suggests open water with lower backscatter than in W1, possibly due to presence of new ice. Air temperature was

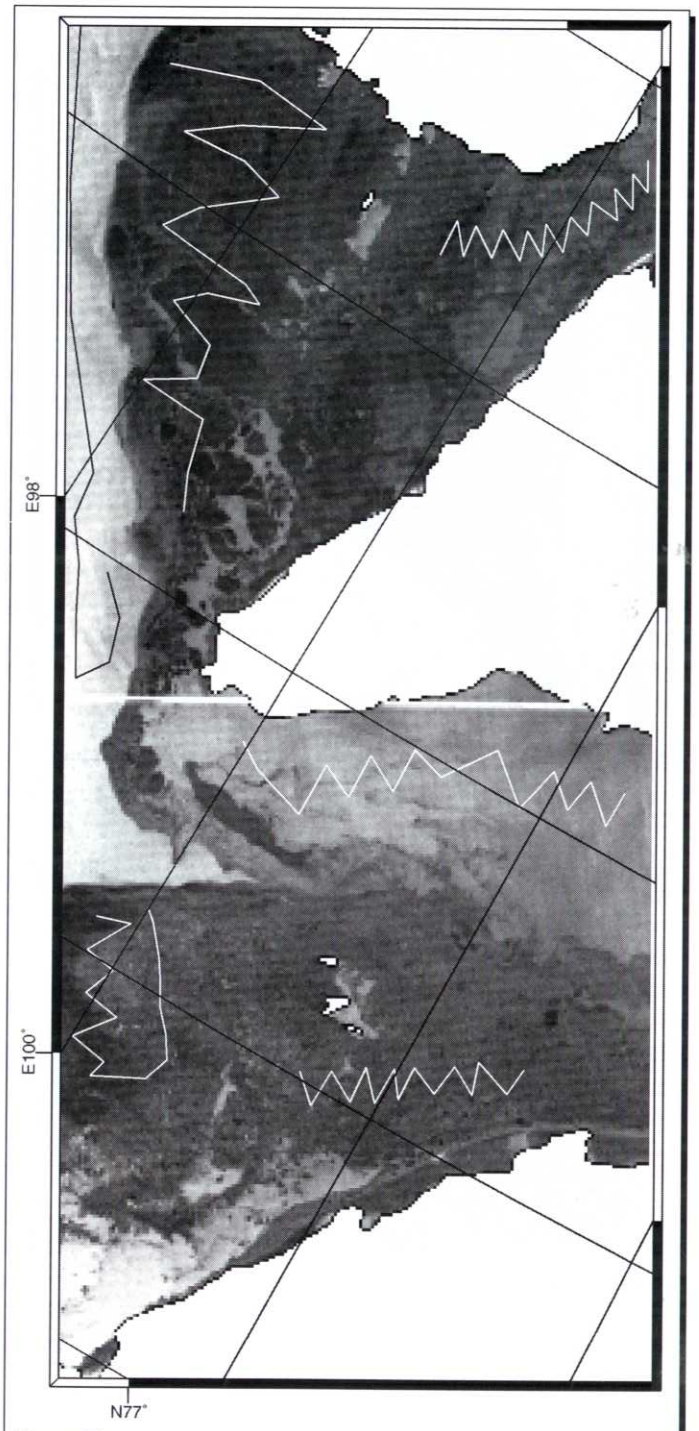

Figure 11a.
With 11b, near simultaneous SAR coverage by ERS-2 of western Vilkitsky Strait and Shokalsky Strait on August 14 1997. The images were obtained at 1354 GMT for ERS-2. The images are put into a common geographical coordinate system with a land mask superimposed. The zigzag lines represent profiles of pixels which were compared between the two images and presented in Figure 12. ©ESA/TSS and Canadian Space Agency, 1997.

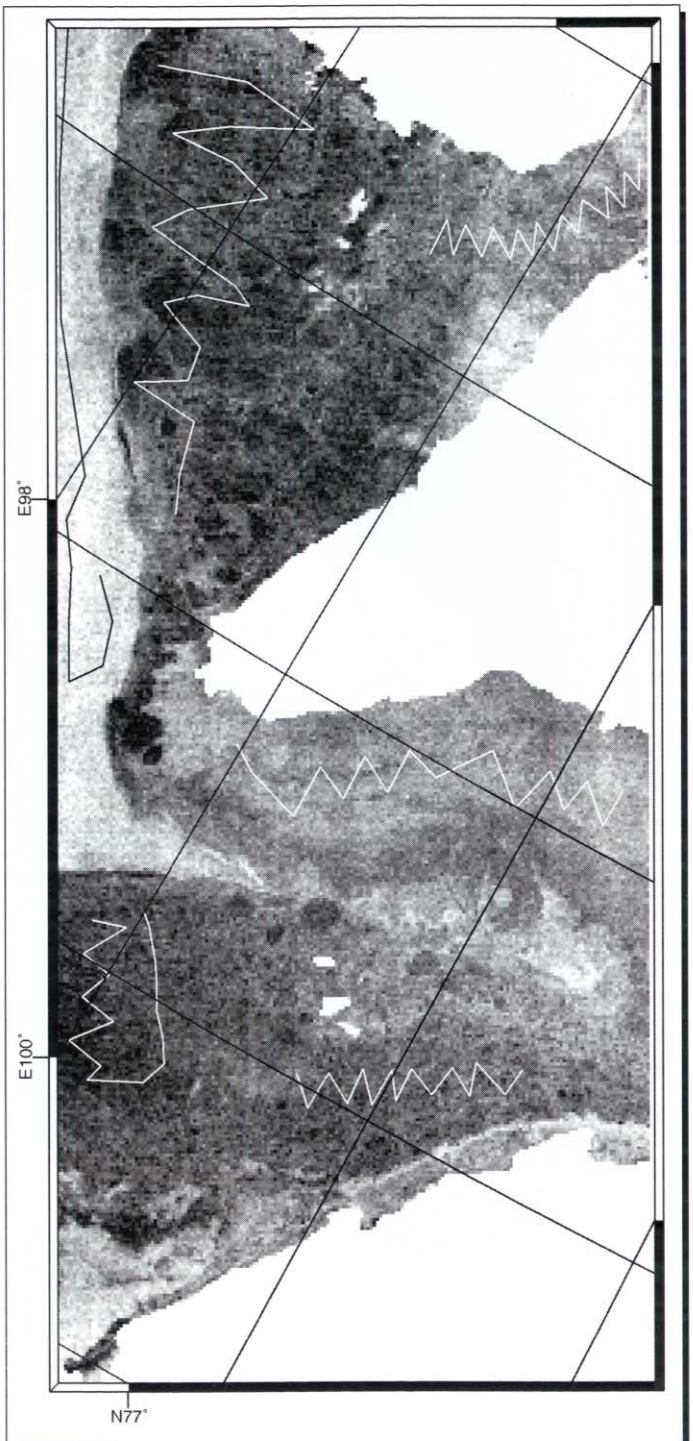

Figure 11b.
With 11a, near simultaneous SAR coverage by RADARSAT of western Vilkitsky Strait and Shokalsky Strait on August 14 1997. The images were obtained at 0933 GMT for RADARSAT. The images are put into a common geographical coordinate system with a land mask superimposed. The zigzag lines represent profiles of pixels which were compared between the two images and presented in Figure 12. ©ESA/TSS and Canadian Space Agency, 1997.

constantly between 0 and -2°C in this period according to the ECMWF data and water temperature was assumed to be at freezing point. This is due to the observation that the surface water in this area was transported southward along the western

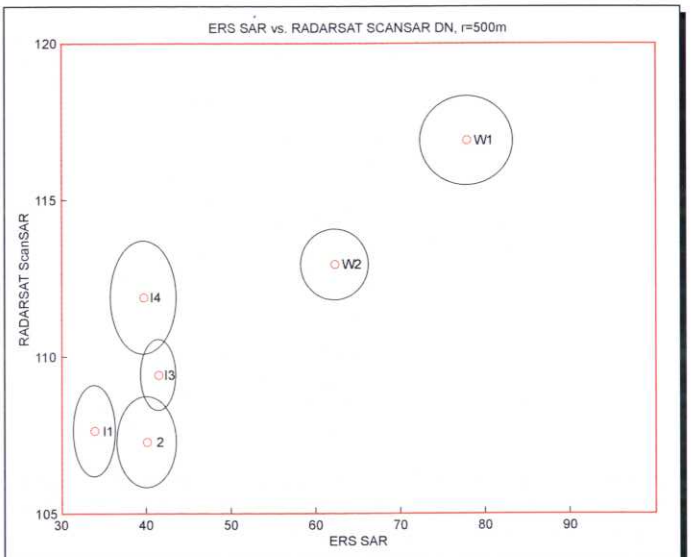

Figure 12.
Pixel-by-pixel comparison of ERS and RADARSAT images based on digital values of the profiles indicated in the images in Figure 11. W1 is the open water profile along the left side of the images; W2 is in the northern part of the Vilkitsky Strait; I1 and I4 is in the outer and inner part of Shokalsky Strait, respectively, while I2 and I3 are in the centre and western part of the southern Vilkitsky Strait.

side of Severnaya Zemlya, where ice cover will keep the surface temperature at the freezing point. The RADARSAT image shows a signature more similar to ice-covered areas such as the southern part of the Vilkitsky strait (I2) or the Shokalsky strait (I4). The ice which drifts into the southern part of the Vilkitsky Strait (I2) and (I3) is assumed to consist mainly of ice which has survived the summer in the Nordenskiold archipelago. As this ice breaks up in late summer it drifts eastward with the currents. RADARSAT seems to be able to discriminate between I2 and I3, while ERS-2 shows similar backscatter for the two areas. RADARSAT also appears to discriminate between the ice in the southern Vilkitsky Strait (I2 and I3) and in the Shokalsky strait (I4) while ERS-2 does not. The ice drifting southward from the west coast of October Revolution Island (I1) has darker signatures than the other ice areas in the ERS-2 image, while RADARSAT shows similar backscatter between I1 and I2. All four ice areas (I1 - I4) are assumed to be fast ice from the previous winter is in the stage of breaking up and drifting away mainly through the Vilkitsky Strait.

Some specific small features, which are not included in the quantitative comparison in **Figure 12**, show pronounced differences between the two SAR systems: the lee side of the small islands in the Shokalsky strait (78° 40'N 98°-99°E) show bright signature in the ERS-2 image due to open water in a wind-generated polynya while the signature in the RADARSAT image is dark. In the Vilkitsky Strait, a similar open polynya near the small islands at 77° 40'N, 101°-102°E is evident in the ERS-2 image but has no distinct signature in the RADARSAT image. The RADARSAT image shows brighter areas in Shokalsky Strait (78° 30'N, 100°E) and in Vilkitsky Strait (77°50'N, 103°E), which are not evident in the ERS-2 images. There are no available *in situ* observations which can confirm

these differences between RADARSAT and ERS-2 signatures.

The higher variability of RADARSAT backscatter compared to ERS-2 for I2, I3 and I4 can be caused by the different amount of water that is included in the ice pixels for the three areas. While homogeneous summer ice should have near-constant values around a given point in the diagram, water has a different response in the two sensors, both as function of wind speed at a given range, and of different distances in range-direction. As open water in case W1 has higher backscatter than ice, it can be concluded that I4 contains more open water and I2 has less open water within the pixels.

Ice Concentration Analysis

Ice concentration is one of the key quantitative parameters, important for ice navigation, which can be derived from RADARSAT ScanSAR images at a significantly higher resolution than SSM/I ice concentration maps. Several investigators have suggested methods for retrieving ice concentration from SAR images (Askne and Ulander, 1992; Dokken *et al.*, 2000; Shokr *et al.*, 1999), but there have not yet been established standard algorithms for wide use. Especially during summer conditions when the ice surface is wet from melting and can be difficult to distinguish from open water, it is a challenge to develop reliable algorithms for retrieving ice concentration from SAR data.

A method to estimate total ice concentration in the ScanSAR image of September 7 has been tested using input from SSM/I observations of the same day. The first assumption of the method is that a threshold value separating ice from open water in leads in the ice-cover can be found in a SAR image without absolute calibration. However, range-correction must be in place to ensure that the water-ice discrimination is possible across the whole image using the same threshold value. It is well known that with increasing wind speed the SAR backscatter of open water rapidly attains higher values than for ice. The next assumption is that within the ice-cover, water pixels will have a lower backscatter value than ice pixels, at least for the images analyzed in this study. However, sufficient high winds can occur in leads to generate higher backscatter than for the ice types. In such cases, the method also has to use an upper threshold to discrimate high backscatter open leads from ice with lower backscatter. Close to the ice edge and within leads and polynyas, the assumption that a lower and upper threshold can discriminate water from ice can also fail. Such areas can nevertheless easily be identified in the SAR image and then masked out.

The pixel size of the original ScanSAR image was first reduced from 50 m to 500 m in order to reduce the speckle noise. After all land areas had been removed from the image, open water regions were determined and masked out using ice concentrations estimated from SSM/I, obtained by the updated NORSEX algorithm (Svendsen *et al.*, 1983). A threshold of 20% ice cover was used for this operation. By analyzing the histogram of the remaining SAR-pixels, two distinct peaks were found, assuming to correspond to ice and water areas, respectively, within the ice-cover. The pixel-value at the local minimum between the two peaks was chosen as the threshold value for separating the two surface types. In the next step all pixels with value above the threshold was set to 100 and all other pixels to 0, *i.e.*, 100% or 0% ice concentration. Using SAR data, ice concentration could be estimated over a certain unit area, defined by n by n pixels. The ice concentration was thus estimated at a resolution of 6.5 km, simply by computing the average mean over 13 by 13 pixels. The results of the analysis of the SAR image of September 7 is shown in **Figure 13a**, while the SSM/I concentration for the same day is shown in **Figure 13b**. The figure shows that ice concentration can be mapped in detail with SAR data, while the SSM/I data will smear out all details less than 10 - 20 km.

One aspect of a simple thresholding procedure is the fact that newer ice types such as grease ice, nilas and gray ice also have relatively low backscatter signatures (Sandven *et al.*, 1999), similar to calm open water. This means that in several cases these ice types will be classified as open water, and as a result the ice concentration will be estimated only on the basis of first-year ice and other ice types with backscatter signatures above the threshold value (including ridged young ice). For many practical purposes, including navigation and estimation of heat flux, this is not a severe drawback. Nevertheless, quantitative analysis should be carried out in order to assess the performance of various SAR ice concentration methods.

The performance of the SAR ice concentration algorithm was analyzed by comparing the resulting ice concentration map with an SSM/I derived ice concentration map. A linear regression analysis performed on a profile extracted from the two data sets, containing altogether 328 pixels, showed a correlation of 0.76 and a RMS of 12.4. The profiles are shown in **Figure 14a**. It can be seen that although the two data sets agree fairly well on an overall basis, the RADARSAT algorithm tends to overestimate the ice concentration compared to SSM/I data. Taking into account the difference between SAR and SSM/I data, both radiometrically and in spatial resolution, it is not surprising that the two data sets give somewhat different results.

Another validation exercise was performed by comparing the SSM/I ice concentration with *in situ* observations from I/B Yamal shown in the **Figure 10a**. A profile of SSM/I and *in situ* observations of ice concentration is shown in **Figure 14b**, indicating that the SSM/I data agrees well with *in situ* observations for this particular case. Discrepancies between the two data types, as seen by the single *in situ* point which is far from the SSM/I estimate in **Figure 14b**, can be ascribed to the difference in resolution in the two observation methods. The coarse resolution in SSM/I data does not necessarily reflect smaller scale and local features which are captured by *in situ* observations. Another element is the standard of *in situ* observations taken on routinely basis onboard icebreakers, which is not necessarily of scientific quality.

Discussion and Conclusions

The analysis of a sequence of ERS-2 and RADARSAT SAR images during late summer conditions shows that the ice motion in the Laptev Sea area is mainly directed in a south-southeasterly

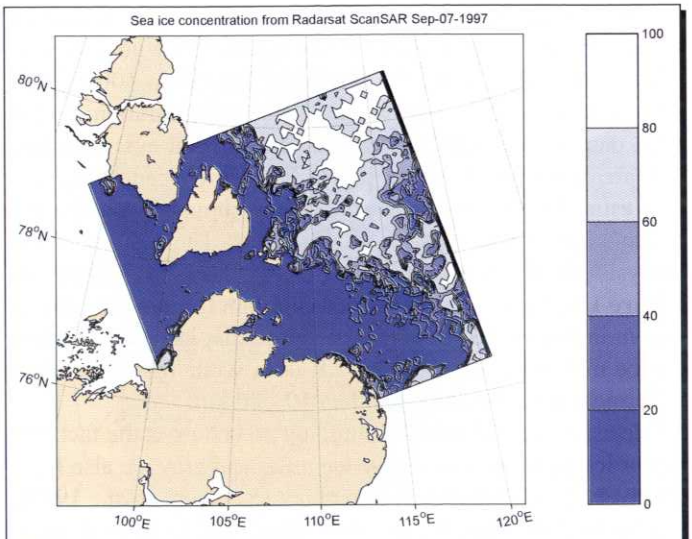

Figure 13a.
Ice concentration analysis of the ScanSAR image of September 4, presented with a spatial resolution of about 6 km.

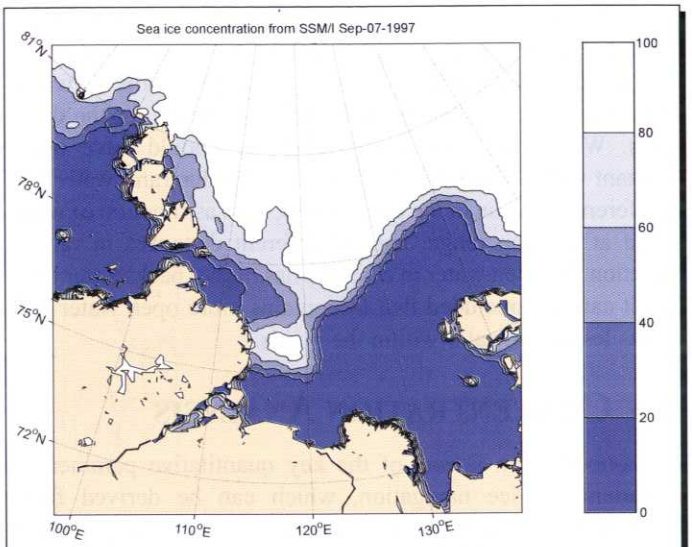

Figure 13b.
Ice concentration estimated from SSM/I data on the same day using the NORSEX algorithm (Svendsen et al., 1983) with the 85 GHz channel.

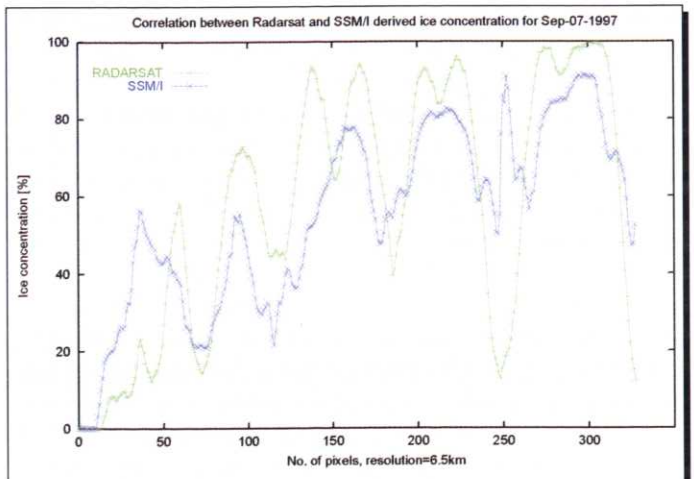

Figure 14a.
Coinciding profiles of ice concentration obtained from ScanSAR data and SSM/I data shown in Figure 13. The profile, which is about 300 km long, is a combination of several shorter profiles cutting across the ice edge and penetrating into the compact ice massif several places in the image.

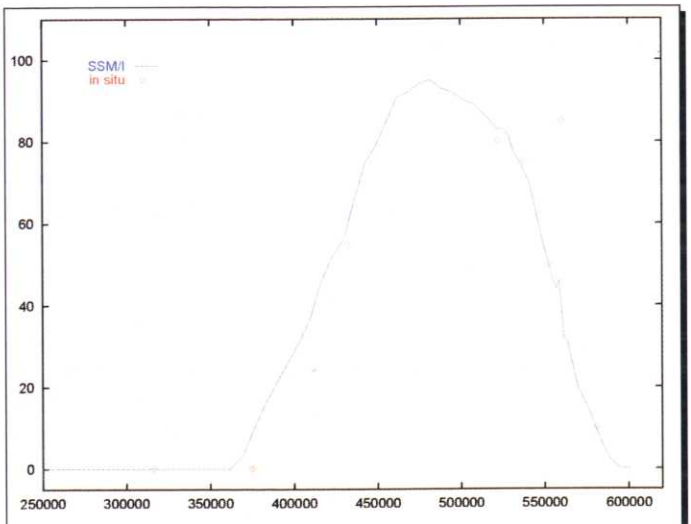

Figure 14b.
Profile of SSM/I ice concentration from a profile taken along the points of *in situ* observations shown in Figure 10a. The ice concentration from the *in situ* observations are indicated by the dots. Units along x-axis are metres in west-east direction and y-axis is concentration in %.

direction and that the ice drifts eastward through the Vilkitsky Strait (**Figure 15**). A few images from the area around the New Siberian Island suggest easterly drift north of 76°N while it turns westerly between 76°N and the mainland. Westerly ice drift was also observed in Sannikov Strait, transporting ice from East Siberian Sea into the Laptev Sea. The prevailing winds were westerly, but wind speeds were low typical less than 10 ms^{-1} over the whole period. The SAR imagery showed unique capability for mapping ice drift in straits and near coasts where other methods provide very little information.

In addition to describing dynamic features of the ice cover, we have attempted to compare RADARSAT and ERS signatures of the same areas, analyze SAR backscatter to classify ice-water areas and derive ice concentration. The *in situ* observations obtained from the nuclear icebreakers Sovetsky Soyuz and Yamal have been used to validate ice types and ice phenomena observed in the SAR images. First-year ice which has survived the summer melt season and is in the stage of transiting to second-year ice, has been well identified in the SAR images, except when concentration goes below 10%. New ice types such as grease ice, nilas and young ice have been difficult to separate from open water in cases when the wind is low (< 5 ms^{-1}).

More systematic backscatter analysis of all SAR images has not been done due to lack of calibrated SAR images. By using SSM/I data to remove high backscatter areas in open water, it has been possible to determine a threshold value between ice

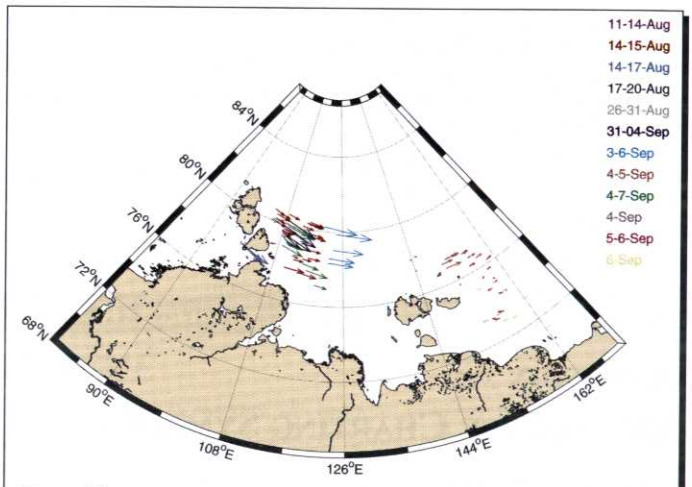

Figure 15.
Composite of all ice drift estimates from successive SAR images analyzed for the period from August 11 to September 7, 1997.

and open water signatures within the ice pack, which has been the basis for estimating ice concentration in a ScanSAR image. By use of SSM/I data within the ice pack, the SAR ice concentration estimates could be validated. *In situ* ice concentration observations from icebreakers were used to validate the SSM/I ice concentration due to lack of coincident *in situ* and SAR data. The most critical step in ice concentration estimation is to distinguish open water from various ice types in a robust manner. Further development of SAR ice concentration methods are needed, taking into account that open water can attain a wide range of backscatter depending on the wind speed. Ice concentration from SAR images can improve the resolution significantly, which is useful in many applications, from ice navigation to calculation of heat flux through leads.

The study has shown that RADARSAR ScanSAR data can be successfully used to observe summer ice conditions in the Northern Sea Route where accurate ice data are essential for safe and cost-effective navigation. The expedition with I/B Sovetsky Soyuz to the Laptev Sea in September 1997 was the first opportunity to test use of RADARSAT ScanSAR images in this region and demonstrate applicability in summer ice navigation. SAR images for the Vilkitsky Strait area, including both RADARSAT and ERS-2, were ordered for delivery in near-real time from Tromsø Satellite Station, and were transmitted in digital form to I/B Sovetsky Soyuz during her voyage to the Laptev Sea. Since the INMARSAT system does not cover the Laptev Sea area, images were transmitted to the icebreaker while sailing in the Kara Sea. When the icebreaker arrived in the ice region, the SAR images had already been analyzed onboard and the sailing route planned. The conclusion of this first exercise with RADARSAT images to support ice navigation in the Vilkitsky Strait and western Laptev Sea was that SAR data is a very useful supplement to traditional ice maps. In this region where ship traffic depends heavily on good quality ice data, the ice conditions are not very well known and SAR data can contribute significantly to better ice information.

Acknowledgements

RADARSAT SAR data were provided through the ADRO-Project N259 and NASA/ASF. The ERS SAR data have been provided by ESA through the ICEWATCH Project. Support to data purchase and analysis has also been given by the IMSI project funded by EU (contract no. ENV4-CT96-0361). Murmansk Shipping Company's Icebreaker Fleet, and in particular the crews onboard I/B Sovetsky Soyuz and I/B Yamal are acknowledged for their excellent support during field observations and demonstration of SAR data transmission.

References

Abramov, V. (1996). *Atlas of Arctic Icebergs, The Greenland, Barents, Kara, Laptev, East-Siberian and Chukchi Seas and the Arctic Basin*. Backbone Publishing Company.

Alexandrov, V.Y., Martin, T., Kolatschek, J., Eicken, H., Kreyscher, M. and Makshtas, A.P. (2000). "Sea Ice Circulation in the Laptev Sea and Ice Export to the Arctic Ocean: Results from Satellite Remote Sensing and Numerical Modeling", *Journal of Geophysical Research*, Vol. 105, No. C7, pp. 17143-17159.

Alexandrov, V.Y., Sandven, S., Johannessen, O.M., Dalen, Ø., and Pettersson, L.H. (2000). "Winter Navigation in the Northern Sea Route". *Polar Record*, Vol. 36 (199), pp. 333-342.

Askne, J. and Ulander, L. (1992). "Remote Sensing of Arctic Sea Ice Using the ERS-1 SAR'. In *Central Symposium of the 'International Space Year' Conference Munich, Germany*, (pp. 129-133). Noordwijk, The Netherlands: ESA Publications Division (ESA SP-341).

Bushuev, A.V., Grishchenko, V.D., and Masanov, A.D. (1985). "Sea Ice Interpretation on Radar Satellite Images", *Issledovanie Zemli iz Kosmosa*, No. 3, pp. 9-15. (in Russian)

Dmitrenko I.A., Gribanov, V.A., Volkov, D.L., Kassens, H., Eicken, H. (1999). "Impact of River Discharge on the Sea Land Fast Ice Extension in the Russian Shelf Area", In J. Tuhkuri and K. Riska (Eds), *The 15th International Conference on Port and Ocean Engineering Under Arctic Conditions,* (Vol. 1, pp. 311-321). Espoo, Finland.

Dokken, S.T., Häkansson B., and Askne, J. (2000). "Inter-Comparison of Arctic Sea Ice Concentration Using RADARSAT, ERS, SSM/I and *In-Situ* Data", *Canadian Journal of Remote Sensing*, Vol. 26, No. 6, pp. 521-536.

Drinkwater, M.R., Kwok, R., Rignot, E., Israelsson, H., Onstott, R.G., and Winebrenner, D.P. (1992). "Potential Applications of Polarimetry to the Classification of Sea Ice", In *Microwave Remote Sensing of Sea Ice*, AGU, Geophysical Monograph 68, eds. F.D.Carsey, chapter 24, pp. 419-430.

Eicken, H., Reimnitz, E., Alexandrov, V., Martin, Th., Kassens, H., Viehoff, Th. (1997). Sea-Ice Processes in the Laptev Sea and Their Importance for Sediment Export, *Continental Shelf Research*, Vol. 17, No. 2, pp. 205-233.

Eicken, H., Alexandrov, V., Bogdanov, V., Martin, T., Reimnitz, E., Syrtsov, S. (1994). Iceberg Observations, *Berichte zur Polarforschung*, Vol. 149, pp. 76-78.

Gill, R.S., Valeur, H.H., and Nielsen, P. (1997). "Evaluation of the RADARSAT Imagery for the Operational Mapping of Sea Ice Around Greenland", In *Geomatics in the era of RADARSAT, GER'97 Symposium*, Ottava.

Gudkovich, Z., M., Kirillov, A.A., Kovalev, E.G., Smetannikov, A.V., Spichkin, V.A. (1972). *The Basis of Techniques for Long-Term Ice Forecasts in the Arctic Seas.* Leningrad: Gidrometeoizdat (in Russian).

Govorukha, L.S. (1988). *Sovremennoe nazemnoye oledenenie Sovetskoy Arktiki (modern glaciation of the Soviet Arctic)*. Leningrad: Gidrometeoizdat.

Johannessen, O.M., Sandven, S., Budgell, W.P., Johannessen, J.A., and Shuchman, R. (1994). "Observation and Simulation of Ice Tongues and Vortex-Pairs in the Marginal Ice Zone". *Nansen Centennial Volume*. American Geophysical Union Monograph 85.

Johannessen, O.M., Sandven, S., Kloster, K., Pettersson L.H., Melentyev V.V., Bobylev, L.P., and Kondratyev, K.Ya. (1997). "ERS-1/2 SAR Monitoring of Dangerous Ice Phenomena Along the Western Part of Northern Sea Route", *International Journal of Remote Sensing*, Vol. 18, No. 12, pp. 2477-2481.

Johannessen, O.M., Volkov, A.M., Bobylev, L.P., Grischenko, V.D., Sandven, S., Pettersson, L.H., Melentyev, V.V., Asmus, V., Milekhin, O.E., Krovotyntsev, V.A., Smirnov, V.G., Alexandrov, V.Y., Duchossois, G., Kozlov, V., Kohlhammer, G., and Solaas, G. (2000). "ICEWATCH - Real-Time Sea Ice Monitoring of the Northern Sea Route Using Satellite Radar (a Cooperative Earth Observation Project between the Russian and European Space Agencies)". *Earth Observation and Remote Sensing*, Vol. 16, No. 2, pp. 257 – 268.

Johannessen O.M., Alexandrov V.Y., Sandven S., Pettersson L.H., Bobylev L.P., Khizhnichenko V.M., Volkov A.M., Lundhaug M., Dalen O., Kloster K., Bogdanov A.V., and Zaitsev L.V. (1999). "Synergistic Use of RADARSAT, ERS and "Okean" Radar Images for Sea Ice Studies in the Northern Sea Route". In T.I. Stein (Ed.), *IEEE 1999 International Geoscience and Remote Sensing Symposium (pp. 1570-1572)*. Hamburg: The Institute for Electrical and Electronics Engineers, Inc.

Kolatschek, J., Viehoff, T., Eicken, H., Nagelsbach, E., and Alexandrov, V. (1995). "Ice Dynamics in the Southwestern Laptev Sea As Derived from ERS-1 SAR Images", *Berichte zur Polarforschung*, Vol. 176, pp. 20-24.

Nghiem, S.V., Martin, S., Perovich, D.K., Kwok, R., Drucker, R., and Gow, A.J. (1997). "A Laboratory Study of the Effect of Frost Flowers on C-Band Radar Backscatter from Sea Ice", *Journal of Geophysical Research*, Vol. 102, No. 2, pp. 3357-3370.

Onstott, R.G. (1992). "SAR and Scatterometer Signatures of Sea Ice". *Geophysical Monograph 68, Microwave Remote Sensing of Sea Ice*. Washington: American Geophysical Union.

RADARSAT. (1997). *Data Products Specifications*, RSI-GS-026, by RADARSAT International, Richmond, Canada.

Ramsay, B.R., Weir, L., Wilson, K., and Arkett, M. (1996). "Early Results of the Use of RADARSAT ScanSAR Sata in the Canadian Ice Service". *The Fourth Symposium on Remote Sensing of the Polar Environments*, (pp. 95-117). Lyngby, Denmark: European Space Agency (ESA SP-391, July 1996).

Reimnitz E., Eicken, H., Martin, T. (1995). "Multiyear Fast Ice along the Taymyr Peninsula, Siberia", *Arctic*, Vol. 48, No. 4, pp. 359-367.

Sandven, S., Alexandrov, V., Lundhaug, M., Kloster, K., and Pettersson, L.H. (1997). "Use of Satellite Synthetic Aperture Radar to Monitor Transport of Pollutants in Sea Ice", *The 3-d International Conference On Environmental Radioactivity in the Arctic*, Tromsø, Norway.

Sandven, S., Maekynen, M., Hallikainen, M., Similae, M., Gronvall, H., Cavanie, A., Ezraty, R., Maroni, C., Gill, R., Valeur, H., Pedersen, L.T., Alexandrov, V.Yu., Andersen, S., Lundhaug, M., Bjorgo, E., Dalen, Ø., and Kloster K., (1998). *Integrated use of new microwave satellite data for improved sea ice observation. IMSI- Development of new satellite ice data products*. (NERSC Technical Rep. No.145). NERSC.

Sandven S., Lundhaug M., Dalen O., Solhaug J., Kloster K., Alexandrov V.Y., Melentyev V.V., and Bogdanov A.V. (1998). "Sea Ice Investigations in the Laptev Sea Using RADARSAT ScanSAR Data". *The International Geoscience and Remote Sensing Symposium (IGARSS'98)* (pp.). Seattle, USA.

Sandven, S, Johannessen, O. M., Miles, M., Pettersson, L.H., and Kloster, K. (1999). "Barents Sea Seasonal Ice Zone Features and Processes from ERS-1 SAR", *Journal of Geophysical Research*, Vol. 104, No. C7, pp. 15843 – 15857.

Shokr, M.R, Jessup, R., and Ramsay, B. (1999). "An Interactive Algorithm for Derivation of Sea Ice Classifications and Concentrations from SAR Images", *Canadian Journal of Remote Sensing*, Vol. 25, No. 1.

Svendsen, E., Kloster, K., Farrelly, B., Johannessen, O.M., Johannessen, J.A., Campbell, W.J., Gloersen, P., Cavalieri, D., and Matzler, C. (1983). "Norwegian Remote Sensing Experiment: Evaluation of the Nimbus 7 Scanning Multichannel Microwave Radiometer for Sea Ice Research", *Journal of Geophysical Research*, Vol. 88, No. C5, pp. 2781-2791.

Zakharov, V.F. (1966). "The Role of Flaw Leads off the Edge of Fast Ice in the Hydrological and Ice Regime of the Laptev Sea", *Oceanology*, Vol. 6, pp. 815-821. (in Russian).

Zakharov, V.F. *Morskie ldy v klimaticheskoi systeme* (Sea ice in the Climate System). St. Petersburg: Gidrometeoizdat (in Russian).

APPENDIX A: RUSSIAN ICE CHARTING SYMBOLS

Symbols	Ice parameters	
	Pack ice concentration, total (tentha) Ice concentration, partial (tentha)	
	Development (age)	**Thickness**
	Grey–white ice (GrW)	15 –30 cm
	Thin first–year ice (WTh)	30 –70 cm
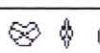	Medium first–year ice (WMd)	70 –120 cm
	Thick first–year ice (WTk)	> 120 cm
	Combination (WMd/WTk)	
	Floe size	**Horizontal sizes**
	Vast floe	2 – 10 km
	Big floe	0.5 – 2 km
	Medium floe[1]	100 –500 m
	Small floe	20 – 100 m
	Small ice cake/brash ice	< 2 m
	Ice age features	**Ice concentration**
	Combination (WMd/WTk, GrW)	9–10 [6 | 3–4]
	Combination (WMd/WTk, GrW)	8–9 [4–5 | 3–4]
	Combination (WTk, WMd, GrW)	7–8 [1–2 | 3 | 3]
	Combination (WMd/WTk, GrW)	7–8
	Combination (WMd/WTk)	4–5
	Combination (WMd/WTk)	1–3
	Ice free	0
	Forms of fast ice	**Thickness**
	Medium	70 – 120 cm
	Thick	> 120 cm
	Thick, brackish water ice	> 120 cm
	Grounded hummock	
	Miscellaneous features	
	Melting stage (0–5)	
	Ridge	

Journal web-site: http://www.casi.ca/index.php?pg=cjrs